HHS Public Access

Author manuscript

Mol Pharm. Author manuscript; available in PMC 2019 July 02.

Published in final edited form as:

Mol Pharm. 2018 July 02; 15(7): 2559–2569. doi:10.1021/acs.molpharmaceut.8b00088.

Multi-arm Nanoconjugates for Cancer Cell-Targeted Delivery of Photosensitizers

Yan Zhao[#1,2], **Fang Li**[#1,3], **Chengqiong Mao**[1], and **Xin Ming**[1,*]

[1]Department of Cancer Biology and Comprehensive Cancer Center, Wake Forest University School of Medicine, Winston-Salem, NC 27157, USA;

[2]National Pharmaceutical Engineering Research Center, China State Institute of Pharmaceutical Industry, Shanghai 201203, China

[3]School of Pharmacy, Jiangsu Vocational College of Medicine, Yancheng 224005, China

[#] These authors contributed equally to this work.

Abstract

Photodynamic therapy, a procedure that uses a photosensitizer to enable light therapy selectively at diseased sites, remains underutilized in oncological clinic. To further improve its cancer selectivity, we developed a polymeric nanosystem by conjugating a photosensitizer IRDye 700DX (IR700) and cancer targeting RGD peptide to 8-arm polyethylene glycol (PEG). The resulting nanoconjugates (RGD-8PEG-IR700) exhibited a hydrodynamic size of 6.6 nm with narrow distribution of size. The targeted nanoconjugates showed significantly higher intracellular uptake of IR700 in integrin αvβ3-expressing A375 and SKOV3 cells when compared with non-targeted control 8PEG-IR700, and excess amount of RGD peptides could abolish this enhancement, indicating a receptor-mediated uptake mechanism for the targeted polymer conjugates. Phototoxicity studies indicated that RGD-8PEG-IR700 produced massive cell killing in A375 cells after photo-irradiation with an IC_{50} value of 57.8 nM of IR700. In contrast, free IR700 and the control 8PEG-IR700 conjugates did not produce any phototoxicity at the concentrations up to 1 μM of IR700. Upon photo-irradiation, the RGD-8PEG-IR700 could produce sufficient singlet oxygen in the cells and induced cell apoptosis. The studies with three-dimensional tumor spheroids showed that they penetrated tumor spheroids deeply and produced strong phototoxicity. Thus, we conclude that the polymer nanoconjugates may provide a promising delivery system for targeted photodynamic therapy of cancers due to their small size, cancer cell specificity, and minimal side effects.

Graphical Abstract

[*]Corresponding author: Dr. Xin Ming, xming@wakehealth.edu, Phone number: 1-336-716-8440.

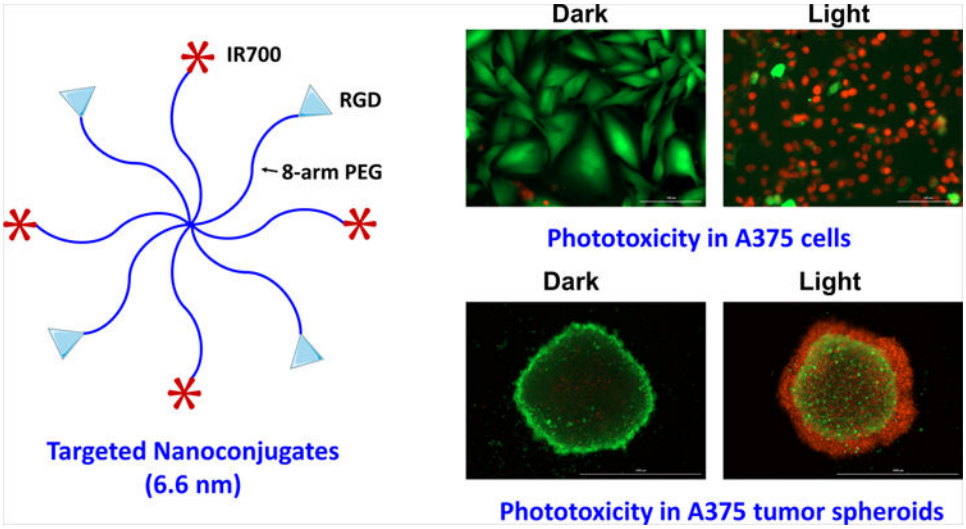

Keywords

photodynamic therapy; multi-arm PEG; nanoconjugates; cancer targeting

1 Introduction

As a clinical cancer treatment, photodynamic therapy (PDT) achieves cancer specific treatment through spatially selective light irradiation.[1] In a typical PDT process, a photosensitizer (PS) is delivered to cancer cells, and then in-tumor irradiation with an appropriate wavelength of light initiates a photochemical reaction, which generates reactive molecular species such as singlet oxygen ($^1O_2$).[1] This causes remarkable phototoxicity and leads to cancer cell death via apoptosis or necrosis. Besides these direct actions on cancer cells, antitumor effects of PDT can derive from damage to the tumor vasculature and development of local and systemic immunity.[1, 2] PDT remains underutilized in oncological practice because of several limitations. Firstly, limited penetration depth of the light prevents its application on solid tumors in deep tissues and metastatic tumors. Further, suboptimal efficacy also comes from intrinsic properties of the PSs, including low solubility, poor cancer uptake, and low extinction coefficients.[3]

One approach to overcome the limitations of conventional PDT is to use nanoparticle (NP)-based delivery of PSs, and thus various nanocarriers, including liposomes, polymeric NPs, and inorganic NPs, have been used to deliver PSs.[4] To load hydrophobic PSs into NPs is a relatively simple process and NPs can enhance the stability of PSs and improve their tumor delivery.[5, 6, 7, 8] Moreover, cancer specificity of PDT can be further enhanced by utilizing novel nanomaterials with temperature-responsive,[9] reactive oxygen species-triggered,[10] or acidity-activatable[11] functionalities. NP-based delivery is often limited by poor penetration in solid tumors,[12] and NPs smaller than 50 nm have better tumor penetration. For example, it was reported that NPs smaller than 20 nm showed greater tumor penetration, and helped produce cytotoxic singlet oxygen deeply in tumors.[13,14] Further, treatment of PS-containing lipidots with the size of 50 nm produced excellent tumor responses after in-tumor light

irradiation.[15] Another potential limitation of NPs is their potential side effects in clinical application. Only a few NP formulations have been tested for clinical applications in human, and thus the long-term side effects of most nanomaterials are still unclear. The potential toxicity of nanomaterials depends on their composition and physicochemical properties,[16] and thus it is important to select safe materials for clinical application of PDT. Polyethylene glycol (PEG) is a US Food and Drug Administration (FDA)-approved polymer that generally does not cause toxicity to humans, and it has been widely used in polymer-based drug delivery. PEG has been used as a carrier to deliver PSs and has shown to enhance tumor delivery of PSs and improve PDT efficacy. [7, 17–20] Multi-arm PEG has higher drug-loading capacity than linear PEG, and it can achieve multiple functionalities when linked to different moieties simultaneously. Multi-arm PEG have been used in the fields of tissue engineering[21, 22] and drug delivery.[23–25]

In order to address the limitations of conventional PDT, we constructed multi-arm nanoconjugates for targeted delivery of PSs to cancer cells. Arg-Gly-Asp (RGD) peptide sequence is a basic unit in cellular recognition and mediates cell binding.[26, 27] RGD peptides bind to several integrin receptors including integrin αvβ3 that is highly expressed in several solid tumors.[28] Therefore, RGD-targeted delivery of PSs is an effective approach to enhance cancer selectivity of PDT.[12, 29] IRDye®700DX (IR700) is a phthalocyanine PS, and is excited in the near-infrared (NIR) range. It has a comparatively higher extinction coefficient and is also more hydrophilic than many PSs.[4] In this study, we conjugated both RGD targeting peptides and IR700 to an 8-Arm PEG molecule simultaneously. Due to multiple arms of the PEG, we could link multivalent tumor-targeting ligands and multiple PS molecules in a single nanoconjugate molecule for enhanced tumor delivery. Further, cellular uptake, generation of reactive oxygen species (ROS), and photokilling of the nanoconjugates were examined in integrin-expressing cancer cells, and their penetration and anticancer activity were investigated with a 3-D tumor spheroids model.

2 Materials and methods

2.1 Preparation of RGD-8PEG-IR700 nanoconjugates

The maleimide group was introduced to a bivalent RGD peptide, H-Glu(cyclo(Arg-Gly-Asp-D-Tyr-Lys))$_2$ (Peptides International, Louisville, KY, USA), by reacting the peptide with N-γ-maleimidobutyryl-oxysuccinimide ester (GMBS, Thermo Fisher Scientific, Rockford, IL, USA) at a 1:3 molar ratio of RGD to GMBS in phosphate buffered saline (PBS, pH7.2) for 30 min at room temperature. The modified RGD-mal was purified with semi-preparative HPLC using an Agilent ZORBAX C18 column (9.4×250 mm, 5 μm, Agilent Technologies, Santa Clara, CA, USA).

The nanoconjugates were synthesized according to the scheme in Figure 1. Briefly, 8-Arm PEG-OPSS (MW: 20K, Creative PEG works, Winston-Salem, NC, USA) was reduced with DTT (50mM) and purified with a Zeba™ Spin Desalting Columns (40K MWCO, Thermo Fisher Scientific). The nanoconjugates were prepared by coupling 8-Arm PEG-SH to RGD-Mal and IR700-mal (LI-COR, Lincoln, NE, USA) at the molar ratio of 1:8:4 in PBS (pH 7.0) containing 5 mM EDTA and the reaction was allowed to proceed for 2 h at room

temperature. The final product was purified with a Zeba™ Spin Desalting Columns (40K MWCO, Thermo Fisher Scientific).

2.2 Characterization of RGD-8PEG-IR700 nanoconjugates

The nanoconjugates were characterized with size-exclusion HPLC using an UltiMate™ 3000 UHPLC system (Thermo Scientific, Dionex, Sunnyvale, CA, USA) equipped with an AdvanceBio SEC-300A column (Agilent Technologies, Inc.) and a diode array detector. All the samples were monitored at the absorbance of 280 nm and 689 nm. The hydrodynamic sizes of the resultant conjugates were measured by dynamic light scattering (DLS) using a Zetasizer Nano (Malvern Instruments, Westborough, MA, USA) at a scattering angle of 90º. To examine singlet oxygen generation (SOG) upon photoirradiation of the nanoconjugates, the mixture of 2 μM singlet oxygen sensor green (SOSG, Thermo Fisher Scientific) and 1 μM IR700 equiv. was prepared. The solution was thereafter irradiated with a 660 nm LED light at the fluent rate of 3.5 mW/cm^2 for 0, 2, 5, 10, 15, and 20 min, respectively. Subsequently, the fluorescence intensity of the solution was measured on a CYTATION 5 imaging reader (BioTeK) at Ex = 504 nm and Em = 525 nm. Meanwhile, the fluorescence intensity of SOSG mixed with PBS, IR700 or 8PEG-IR700 was also determined as controls.

2.3 Cell culture and cellular uptake

Human melanoma cell line A375, human ovarian cancer cell line SKOV3, and mouse fibroblast NIH/3T3 were obtained from ATCC (Manassas, VA, USA). A375 and 3T3 cells were cultured in DMEM medium supplemented with 10% fetal bovine serum (FBS) and 1% penicillin/streptomycin at 37 °C with 5% CO_2. SKOV3 cells were cultured in McCoy's 5A medium supplemented with 10% FBS, and 1% penicillin/streptomycin. To quantify cellular uptake of the nanoconjugates, cells were treated with 8PEG-IR700 or RGD-8PEG-IR700 in the absence and presence of free cRGDfK peptide (10 μM, Peptides International, Inc.) for 4 h. Then the cells were trypsinized to single cells and cell associated fluorescence was analyzed using a BD Accuri™ C6 cytometer (BD, Franklin Lakes, NJ, USA).

2.4 Phototoxicity of RGD-8PEG-IR700 nanoconjugates

A375 cells were incubated with free IR700, 8PEG-IR700 or RGD-8PEG-IR700 at the increasing concentration at 37 °C overnight. Then the cells were washed with fresh medium and photo-irradiated with a 660 nm LED light at the fluent rate of 3.5 mW/cm^2 for 20 min. After 24 h, cell viability was measured using the Alamar Blue Assay as described previously.[12, 30] Briefly, cells were treated with Alamar blue reagent for 4 h, and then the fluorescence was measured at the channel of Ex 540 nm/Em 590 nm on a Cytation5 imaging reader. A375 cells that were treated with the PSs but were not irradiated served as controls.

For live/dead cell staining, A375 cells were treated with 8PEG-IR700 and RGD-8PEG-IR700 (100 nM IR700 equiv) overnight. Six hours after photo-irradiation, the cells were stained with Calcein AM (2 μM) and PI (5 μg/mL) at room temperature for 30 min. Then the cells were imaged with a Cytation5 imaging reader. A375 cells treated with nanoconjugates but not photo-irradiated were used as a control.

2.5 Cellular photoactivity of nanoconjugates

A375 cells were incubated with 8PEG-IR700 or RGD-8PEG-IR700 (100 nM of IR700 equiv.) at 37 °C overnight, and further incubated with 10μM CM-H_2DCFDA (Thermo Fisher Scientific), a general oxidative stress indicator, for 30 min. After replacing with fresh medium, the cells were irradiated with the 660 nm LED light (3.5mW/cm^2) for 20 min. After that, the intracellular ROS production was detected by observing the fluorescent product DCF using a Cytation5 imaging reader. The 8PEG-IR700 nanoconjugates and RGD-8PEG-IR700 without light treatment served as controls.

2.6 Flow cytometry analysis of phototoxicity

After treated with RGD-8PEG-IR700 (100 nM of IR700 equiv.) overnight, A375 cells were photo-irradiated with the 660 nm LED light. After 24 h, the cells were trypsinized, washed, and then stained with Alexa® Fluor 488-labelled Annexin V and PI according to the manufacturer's protocol (Thermo Fisher Scientific). Cellular fluorescence was detected with a BD Canto II flow cytometer (BD, Franklin Lakes, NJ, USA).

2.7 Phototoxicity of RGD-8PEG-IR700 in tumor spheroids

To generate 3D tumor spheroid, 7500 of A375 cells in 200 μL medium per well were seeded into ultra-low attachment 96-well round-bottomed plates (Thermo Fisher Scientific) and cultured for 4 days, and then the three-dimensional structures were achieved. In order to detect the penetration of the conjugates in spheroids, stock dose solution of 8PEG-IR700 or RGD-8PEG-IR700 was added to the spheroids to the final concentrations of 250 nM of IR700 equiv. After overnight treatment, the spheroids were washed with PBS thrice and harvested. Images were taken by confocal laser scanning microscope FV1200 (Olympus Cooperation).

To evaluate the phototoxicity, A375 spheroids were treated with 8PEG-IR700 or RGD-8PEG-IR700 at the concentrations of 500 nM of IR700 equiv. overnight. The spheroids were photo-irradiated with a 660 nm LED light (3.5mW/cm^2) for 30 min. After 24 h, the spheroids were stained with Calcein AM (2 μM) and PI (5 μg/mL) at 37°C for 30 min, and then the images were captured using a Cytation5 imaging reader (BioTek).

Statistical Analysis.

Data were expressed as mean ± SD. Means were compared using Student's t test for two sample comparison or one-way ANOVA followed by Tukey's post-hoc analysis for multiple comparison. *P* values less than 0.05 were considered statistically significant.

3. Results

3.1 Characterization of RGD-8PEG-IR700 nanoconjugates

The SEC-HPLC behaviors of free IR700 and its conjugates are shown in Figure 2A. The 8PEG-IR700 conjugates eluted earlier than IR700 in the column with the retention time of 8.6 and 12.1 min, respectively. The retention time of the RGD-8PEG-IR700 (8.4 min) was little earlier than 8PEG-IR700, due to the slight difference of molecular weight between the two conjugates. The final conjugates only had one peak, which meant that the prepared

conjugates had no free IR700 and the purification was achieved. BSA and IgG were also analyzed in the same SEC-HPLC conditions. As shown Figure 2A, the retention time of RGD-8PEG-IR700 was close to BSA (8.5 min) and shorter than IgG, indicating that the hydrodynamic size of the targeted nanoconjugates is close to albumin (7.6 nm), but smaller than full-length antibody (10 nm). The average hydrodynamic diameter of RGD- 8PEG-IR700 measured by DLS was 6.6 nm (Figure. 2B), which was consistent with the estimation of the SEC-HPLC data. The RGD-to-IR700 ratio of the nanoconjugates was calculated by measurement of their absorption at 280 and 689 nm using UV/Vis spectroscopy. Free RGD peptide and IR700 served as controls. The ratio was determined to be 2.2.

SOSG was used as a probe to determine SOG. The fluorescence intensity of SOSG solutions before and after light treatment is shown in Figure 2C. A fast fluorescence increase was found in all the IR700-containing groups, whereas the PBS group did not show remarkable fluorescence change. The RGD-8PEG-IR700 nanoconjugates showed a comparable $^1O_2$ generation as the other IR700 groups and achieved the peak at 10 min. A gradual decrease was demonstrated in all the IR700 groups after they reached the peak, and the fluorescence of RGD-8PEG-IR700 group dropped faster than the other two IR700 groups in the later 10 min. The results indicated that a type II mechanism is involved in the nanoconjugate-mediated PDT.

3.2 Cellular uptake and serum stability of RGD-8PEG-IR700

Intracellular uptake of 8PEG-IR700 and RGD-8PEG-IR700 was evaluated by treating A375 cells overnight and then measuring IR700 fluorescence intensity using flow cytometry. The results in Figure 3A showed that RGD-8PEG-IR700 exhibited about 109-fold higher intracellular uptake than 8PEG-IR700 in A375 cells. The cRGDfK peptide, a competitive inhibitor of integrin αvβ3 receptor, could dramatically reduce the uptake of RGD-8PEG-IR700, indicating an integrin-mediated endocytosis mechanism. Cellular uptake of the nanoconjugates in integrin αvβ3-negative cell line 3T3 as well as another integrin αvβ3-expressing cell line SKOV3 was also examined. The results in Figure 3 showed that the uptake of RGD-8PEG-IR700 in A375 cells and SKOV3 cells was over 97-fold and 15-fold than that in 3T3 cells, respectively. This data further supports that RGD-8PEG-IR700 enters the cells by integrin-mediated endocytosis.

To examine the serum stability of the targeted nanoconjugates, the RGD-8PEG-IR700 nanoconjugates were incubated in PBS and 20% FBS at 37 °C for a day, and then their cellular uptake in SKOV3 cells was measured using flow cytometry. As shown in Figure 3D, there was not decrease in cellular uptake of RGD-8PEG-IR700 after these treatments, indicating that the nanoconjugates are stable in both PBS and serum.

3.3 Cytotoxicity of RGD-8PEG-IR700

To investigate the cytotoxicity in dark, A375 cells were treated with the PSs at increasing concentrations, and the viability data in Figure 4 showed no dark toxicity of free IR700, control and targeted nanoconjugates up to the concentration of 1000 nM of IR700 equiv. To examine the phototoxicity of free IR700, 8PEG-IR700 and RGD-8PEG-IR700, A375 cells were treated with the PSs at increasing concentrations up to 1000 nM, and then irradiated

with the 660 nm LED light. As shown in Figure 4, almost no cell death was observed when A375 cells were treated by free IR700 or 8PEG-IR700 followed by photo-irradiation. However, after light irradiation, RGD-8PEG-IR700 showed significantly greater phototoxicity to A375 cells than 8PEG-IR700 with an estimated IC_{50} value of 57.8 nM for the targeted nanoconjugates, indicating that targeted nanoconjugates substantially enhance the PDT efficacy.

The phototoxicity of RGD-8PEG-IR700 was confirmed with live/dead cell staining. As shown in Figure 5, after photo-irradiation, most of A375 cells treated with RGD-8PEG-IR700 were killed. In contrast, there was almost no cell damage when the cells treated by RGD-8PEG-IR700 or 8PEG-IR700 without photo-irradiation, or 8PEG-IR700 with light treatment, indicating that intracellular uptake is necessary for IR700 to produce phototoxicity.

3.4 Cellular photoactivity of RGD-8PEG-IR700

Singlet oxygen production upon photo-irradiation of RGD-8PEG-IR700 inside of A375 cells was detected with an oxidative stress indicator CM-H_2DCFDA. This molecule itself is non-fluorescent. After passively diffusing into cells, CM-H_2DCFDA undergoes deacetylation by esterases and subsequent oxidation by reacting with singlet oxygen or other ROS, and finally yields a green fluorescent product that remains trapped within the cells. As shown in Figure 6, bright green fluorescence was only observed in the cells after RGD-8PEG-IR700 treatment followed by photo-irradiation, but in the other cases the singlet oxygen generation was barely detectable, suggesting that photo-irradiation of intracellular RGD-8PEG-IR700 produces singlet oxygen and further triggers cell death events in A375 cells.

3.5 Death pathway analysis of RGD-8PEG-IR700 photokilling

Cell death pathway of RGD-8PEG-IR700 mediated photokilling was determined using Annexin V and PI staining to differentiate among viable (Annexin V^-/PI^-; lower left quadrant), early apoptotic (Annexin V^+/PI^-; lower right quadrant), necrotic (Annexin V^-/PI^+; upper left quadrant), and late apoptotic/secondary necrotic (Annexin V^+/PI^+; upper right quadrant) cells. As shown in Figure 7, about 92% of the cells were viable in the PBS group, while in the RGD-8PEG-IR700 treatment group, there were 37.9% early apoptotic cells and 55.4% late apoptotic and dead cells, respectively, indicating that A375 cells mainly undergo apoptosis upon RGD-8PEG-IR700 mediated photokilling.

3.6 Phototoxicity of RGD-8PEG-IR700 in tumor spheroids

Penetration of non-targeted conjugates (8PEG-IR700), targeted nanoconjugates (RGD-8PEG-IR700), and a polyplexes formulation reported previously[30, 31] were examined in A375 tumor spheroids. As shown in Figure 8, almost no 8PEG-IR700 conjugates were observed even in cells on the surface of the spheroids, while the RGD-8PEG-IR700 could penetrate throughout the spheroid. Additionally, the PEI polyplexes (336 nm in size[30, 31]) could only reach the cells on the surface of spheroids. This result supports the notion that smaller NPs show superior penetration behavior into tumor spheroids than larger NPs.[32]

Compared with 8PEG-IR700, RGD-8PEG-IR700 significantly increased cell death all over the spheroids after light treatment (Figure 9), indicating that RGD-8PEG-IR700 could penetrate the spheroids deeply and produce significant phototoxicity. In contrast, in dark, either of the both nanoconjugates barely generated cell death. This confirmed that the targeted RGD-8PEG-IR700 conjugates is not toxic in dark.

4. Discussion

Clinical PDT has been limited by intrinsic limitations of PSs. In this study, we prepared monomolecular nanoconjugates of PSs to overcome the limitations of conventional PSs that are currently used in oncologic clinic. The polymeric nanoconjugates are small, highly cancer specific, and no dark toxicity, and thus may provide an effective drug delivery system for PDT of cancers.

The core component of the targeted nanoconjugates in this study is the carrier of 8-arm PEG. This multi-arm polymer retains the advantages of conventional PEG as drug carriers, including good water solubility and excellent safety for *in vivo* applications. Due to the multi arms in the polymer, 8-arm PEG has higher capacity to load drug than traditional linear PEG, and its larger hydrophilic portion increases the solubility of nanodrugs.[23] The 8-arm PEG based nanocarriers also shows a more compact structure and a better stability than those from the 4-arm PEG *in vitro*.[22] Compared with 4-arm PEG, 8-arm PEG also shows a better control of mechanical properties. The 8-arm PEG formed hydrogel in a faster manner, and allowed a greater degree of modification without affecting the degrees of swelling and storage modulus when compared to 4-arm PEG.[33] Unlike another type of branched molecules, dendrimers, which have multi-amino groups, 8-arm-PEG shows little toxicity and thus is biocompatible. Moreover, 8-arm-PEG can protect drugs from liver metabolism and improve their bioavailability. A recent study showed that 8-arm-PEG had higher inhibitory activities towards Cytochrome P450 than linear-PEG, 4-arm-PEG, and poly (l-lysine).[34]

Multi-arm PEGs have been used in drug delivery. For example, 4-arm PEG[35], 6-arm PEG[36, 37] and 8-arm PEG[23, 32] have been used in various polymeric delivery system such as hydrogels, micelles, and NPs. However, they have not been used as monomolecular carriers. In this study, we used 8-arm PEGs as monomolecular carriers for cancer targeted delivery of drugs, and the results demonstrated several advantages of our system over other carriers. The first advantage is a small monomolecular size (6.6 nm). The small size led to greater penetration of the targeted nanoconjugates than larger conventional polymer NPs in a tumor spheroid model (Figure 8), and this greater deliver resulted in superior anticancer activity in this 3D tumor model (Figure 9). In addition, the size of the nanoconjugates can be fine-tuned by using polymers with different molecular weights, potentially leading to the nanoconjugates with different circulation half-lives. Thus, the pharmacokinetics of the delivered drugs can be optimized using multi-arm nanoconjugates as drug carriers.

Another advantage of 8-arm PEG as drug carrier is multi-functionality of the targeted nanoconjugates. One limitation of linear PEG is that there are only two functional groups per PEG molecule. There are 4-folded functional groups in an 8-arm PEG molecule and so it’s possible to carry multiple targeting ligands and drug molecules in a single molecule of

PEG. It has been reported that displaying multivalent targeting ligands on the surface of a NP can dramatically enhance receptor binding and lead to superior receptor-mediated cellular uptake.[38] The targeted nanoconjugates displayed over 100-fold enhancement in receptor-specific uptake of the PS in cancer cells compared to the non-targeted control conjugates (Figure 3), indicating that the targeted nanoconjugates are highly cancer selective due to the multivalent presentation of cancer targeting ligands. Minimal cellular uptake of 8-arm PEG itself also contributes to cancer cell selectivity. In a previous study, we linked RGD peptides to PAMAM dendrimers to prepare targeted nanoconjugates, and they only showed 4.7-fold greater uptake than non-targeted PAMAM conjugates.[12] This was due to high cellular uptake of positively charged PAMAM polymers themselves. Comparing these two delivery systems, 8-arm PEG based nanoconjugates may be a better choice for delivery of highly potent chemotherapy agents, which may cause serious side effects when delivered in a non-selective way. In this study, we are able to incorporate two types of functionalities to 8-Arm PEG. In the future, novel polymers or other materials should be developed to incorporate additional moieties for a superior delivery system for targeted cancer therapy.

In conclusion, we successfully developed targeted nanoconjugates of IR700 using 8-arm PEG. The RGD functionalized conjugates substantially enhance cancer cell specific uptake of PSs, generate sufficient singlet oxygen to induce apoptosis of A375 cells upon photo-irradiation, but are non-toxic in dark. In addition, the targeted nanoconjugates are able to penetrate tumor spheroids deeply. Therefore, the multi-arm nanoconjugates may provide a promising drug delivery system for targeted PDT of solid tumors because of their small size and outstanding cancer cell targeting.

Acknowledgements

This study was supported by NIH Grant R01CA194064 (XM). Fang Li was supported by Natural Science Foundation in Colleges of Jiangsu Province No 17KJB350015. We also acknowledge the experimental assistances of the Flow Cytometry Shared Resource that is supported by the Comprehensive Cancer Center of Wake Forest Baptist Medical Center, NCI CCSG P30CA012197 grant.

References

1. Agostinis P; Berg K; Cengel KA; Foster TH; Girotti AW; Gollnick SO; Hahn SM; Hamblin MR; Juzeniene A; Kessel D; Korbelik M; Moan J; Mroz P; Nowis D; Piette J; Wilson BC; Golab J Photodynamic therapy of cancer: an update. CA: a cancer journal for clinicians 2011, 61, (4), 250–81. [PubMed: 21617154]
2. Mallidi S; Anbil S; Bulin AL; Obaid G; Ichikawa M; Hasan T Beyond the Barriers of Light Penetration: Strategies, Perspectives and Possibilities for Photodynamic Therapy. Theranostics 2016, 6, (13), 2458–2487. [PubMed: 27877247]
3. Lim CK; Heo J; Shin S; Jeong K; Seo YH; Jang WD; Park CR; Park SY; Kim S; Kwon IC Nanophotosensitizers toward advanced photodynamic therapy of Cancer. Cancer letters 2013, 334, (2), 176–87. [PubMed: 23017942]
4. Mitsunaga M; Ogawa M; Kosaka N; Rosenblum LT; Choyke PL; Kobayashi H Cancer cell-selective in vivo near infrared photoimmunotherapy targeting specific membrane molecules. Nature medicine 2011, 17, (12), 1685–91.
5. Lee J; Kim J; Jeong M; Lee H; Goh U; Kim H; Kim B; Park JH Liposome-based engineering of cells to package hydrophobic compounds in membrane vesicles for tumor penetration. Nano Lett 2015, 15, (5), 2938–44. [PubMed: 25806671]

6. Nguyen HT; Tran TH; Thapa RK; Pham TT; Jeong JH; Youn YS; Choi HG; Yong CS; Kim JO Incorporation of chemotherapeutic agent and photosensitizer in a low temperature-sensitive liposome for effective chemo-hyperthermic anticancer activity. Expert Opin Drug Deliv 2017, 14, (2), 155–164. [PubMed: 27892715]
7. Lamch L; Tylus W; Jewginski M; Latajka R; Wilk KA Location of Varying Hydrophobicity Zinc(II) Phthalocyanine-Type Photosensitizers in Methoxy Poly(ethylene oxide) and Poly(l-lactide) Block Copolymer Micelles Using 1H NMR and XPS Techniques. J Phys Chem B 2016, 120, (49), 12768–12780. [PubMed: 27973818]
8. Lamch L; Kulbacka J; Pietkiewicz J; Rossowska J; Dubinska-Magiera M; Choromanska A; Wilk KA Preparation and characterization of new zinc(II) phthalocyanine - Containing poly(l-lactide)-b-poly(ethylene glycol) copolymer micelles for photodynamic therapy. J Photochem Photobiol B 2016, 160, 185–97. [PubMed: 27113446]
9. Park W; Park SJ; Cho S; Shin H; Jung YS; Lee B; Na K; Kim DH Intermolecular Structural Change for Thermoswitchable Polymeric Photosensitizer. J Am Chem Soc 2016, 138, (34), 10734–7. [PubMed: 27535204]
10. Cao ZY; Ma YC; Sun CY; Lu ZD; Yao ZY; Wang JX; Li DD; Yuan YY; Yang XZ ROS-Sensitive Polymeric Nanocarriers with Red Light-Activated Size Shrinkage for Remotely Controlled Drug Release. Chem Mater 2018, 30, (2), 517–525.
11. Gao M; Fan F; Li D; Yu Y; Mao K; Sun T; Qian H; Tao W; Yang X Tumor acidity-activatable TAT targeted nanomedicine for enlarged fluorescence/magnetic resonance imaging-guided photodynamic therapy. Biomaterials 2017, 133, 165–175. [PubMed: 28437627]
12. Yuan A; Yang B; Wu J; Hu Y; Ming X Dendritic nanoconjugates of photosensitizer for targeted photodynamic therapy. Acta biomaterialia 2015, 21, 63–73. [PubMed: 25900441]
13. Perry JL; Reuter KG; Luft JC; Pecot CV; Zamboni W; DeSimone JM Mediating Passive Tumor Accumulation through Particle Size, Tumor Type, and Location. Nano Lett 2017.
14. Jeong K; Park S; Lee YD; Kang CS; Kim HJ; Park H; Kwon IC; Kim J; Park CR; Kim S Size-engineered biocompatible polymeric nanophotosensitizer for locoregional photodynamic therapy of cancer. Colloids Surf B Biointerfaces 2016, 144, 303–10. [PubMed: 27107384]
15. Hinger D; Navarro F; Kach A; Thomann JS; Mittler F; Couffin AC; Maake C Photoinduced effects of m-tetrahydroxyphenylchlorin loaded lipid nanoemulsions on multicellular tumor spheroids. J Nanobiotechnology 2016, 14, (1), 68. [PubMed: 27604187]
16. Sharifi S; Behzadi S; Laurent S; Forrest ML; Stroeve P; Mahmoudi M Toxicity of nanomaterials. Chem Soc Rev 2012, 41, (6), 2323–43. [PubMed: 22170510]
17. Roh YJ; Kim JH; Kim IW; Na K; Park JM; Choi MG Photodynamic Therapy Using Photosensitizer-encapsulated Polymeric Nanoparticle to Overcome ATP-Binding Cassette Transporter Subfamily G2 Function in Pancreatic Cancer. Mol Cancer Ther 2017.
18. Boix-Garriga E; Acedo P; Casado A; Villanueva A; Stockert JC; Canete M; Mora M; Sagrista ML; Nonell S Poly(D, L-lactide-co-glycolide) nanoparticles as delivery agents for photodynamic therapy: enhancing singlet oxygen release and photototoxicity by surface PEG coating. Nanotechnology 2015, 26, (36), 365104. [PubMed: 26293792]
19. Timor R; Weitman H; Waiskopf N; Banin U; Ehrenberg B PEG-Phospholipids Coated Quantum Rods as Amplifiers of the Photosensitization Process by FRET. ACS Appl Mater Interfaces 2015, 7, (38), 21107–14. [PubMed: 26334672]
20. Jia HR; Jiang YW; Zhu YX; Li YH; Wang HY; Han X; Yu ZW; Gu N; Liu P; Chen Z; Wu FG Plasma membrane activatable polymeric nanotheranostics with self-enhanced light-triggered photosensitizer cell influx for photodynamic cancer therapy. J Control Release 2017.
21. Wang J; Zhang F; Tsang WP; Wan C; Wu C Fabrication of injectable high strength hydrogel based on 4-arm star PEG for cartilage tissue engineering. Biomaterials 2017, 120, 11–21. [PubMed: 28024231]
22. Tan H; DeFail AJ; Rubin JP; Chu CR; Marra KG Novel multiarm PEG-based hydrogels for tissue engineering. Journal of biomedical materials research. Part A 2010, 92, (3), 979–87. [PubMed: 20540093]

23. Liu K; Dai L; Li C; Liu J; Wang L; Lei J Self-assembled targeted nanoparticles based on transferrin-modified eight-arm-polyethylene glycol–dihydroartemisinin conjugate. Scientific Reports 2016, 6, (1).
24. Tang Z; Zhang L; Wang Y; Li D; Zhong Z; Zhou S Redox-responsive star-shaped magnetic micelles with active-targeted and magnetic-guided functions for cancer therapy. Acta Biomater 2016, 42, 232–46. [PubMed: 27373437]
25. Shi C; Guo X; Qu Q; Tang Z; Wang Y; Zhou S Actively targeted delivery of anticancer drug to tumor cells by redox-responsive star-shaped micelles. Biomaterials 2014, 35, (30), 8711–22. [PubMed: 25002267]
26. Ruoslahti E; Pierschbacher MD Arg-Gly-Asp: a versatile cell recognition signal. Cell 1986, 44, (4), 517–8. [PubMed: 2418980]
27. Leahy DJ; Aukhil I; Erickson HP 2.0 A crystal structure of a four-domain segment of human fibronectin encompassing the RGD loop and synergy region. Cell 1996, 84, (1), 155–64. [PubMed: 8548820]
28. Ruoslahti E; Pierschbacher MD New perspectives in cell adhesion: RGD and integrins. Science 1987, 238, (4826), 491–7. [PubMed: 2821619]
29. Li F; Zhao Y; Mao C; Kong Y; Ming X RGD-Modified Albumin Nanoconjugates for Targeted Delivery of a Porphyrin Photosensitizer. Mol Pharm 2017, 14, (8), 2793–2804. [PubMed: 28700237]
30. Ming X; Carver K; Wu L Albumin-based nanoconjugates for targeted delivery of therapeutic oligonucleotides. Biomaterials 2013, 34, (32), 7939–49. [PubMed: 23876758]
31. Ming X; Feng L Targeted delivery of a splice-switching oligonucleotide by cationic polyplexes of RGD-oligonucleotide conjugate. Mol Pharm 2012, 9, (5), 1502–10. [PubMed: 22497548]
32. Pradal C; Grondahl L; Cooper-White JJ Hydrolytically degradable polyrotaxane hydrogels for drug and cell delivery applications. Biomacromolecules 2015, 16, (1), 389–403. [PubMed: 25469767]
33. Kim J; Kong YP; Niedzielski SM; Singh RK; Putnam AJ; Shikanov A Characterization of the crosslinking kinetics of multi-arm poly(ethylene glycol) hydrogels formed via Michael-type addition. Soft Matter 2016, 12, (7), 2076–85. [PubMed: 26750719]
34. Fasinu P; Choonara YE; Kumar P; du Toit LC; Bijukumar D; Khan RA; Pillay V Enhancement of the Oral Bioavailability of Felodipine Employing 8-Arm-Poly(Ethylene Glycol): In Vivo, In Vitro and In Silico Evaluation. AAPS PharmSciTech 2017, 18, (3), 617–628. [PubMed: 27173987]
35. Huang Q; Li D; Kang A; An W; Fan B; Ma X; Ma G; Su Z; Hu T PEG as a spacer arm markedly increases the immunogenicity of meningococcal group Y polysaccharide conjugate vaccine. J Control Release 2013, 172, (1), 382–9. [PubMed: 23511718]
36. Jeong JH; Hong SW; Hong S; Yook S; Jung Y; Park JB; Khue CD; Im BH; Seo J; Lee H; Ahn CH; Lee DY; Byun Y Surface camouflage of pancreatic islets using 6-arm-PEG-catechol in combined therapy with tacrolimus and anti-CD154 monoclonal antibody for xenotransplantation. Biomaterials 2011, 32, (31), 7961–70. [PubMed: 21831422]
37. Choi SW; Lee SH; Mok H; Park TG Multifunctional siRNA delivery system: polyelectrolyte complex micelles of six-arm PEG conjugate of siRNA and cell penetrating peptide with crosslinked fusogenic peptide. Biotechnol Prog 2010, 26, (1), 57–63. [PubMed: 19918765]
38. Montet X; Funovics M; Montet-Abou K; Weissleder R; Josephson L Multivalent effects of RGD peptides obtained by nanoparticle display. J Med Chem 2006, 49, (20), 6087–93. [PubMed: 17004722]

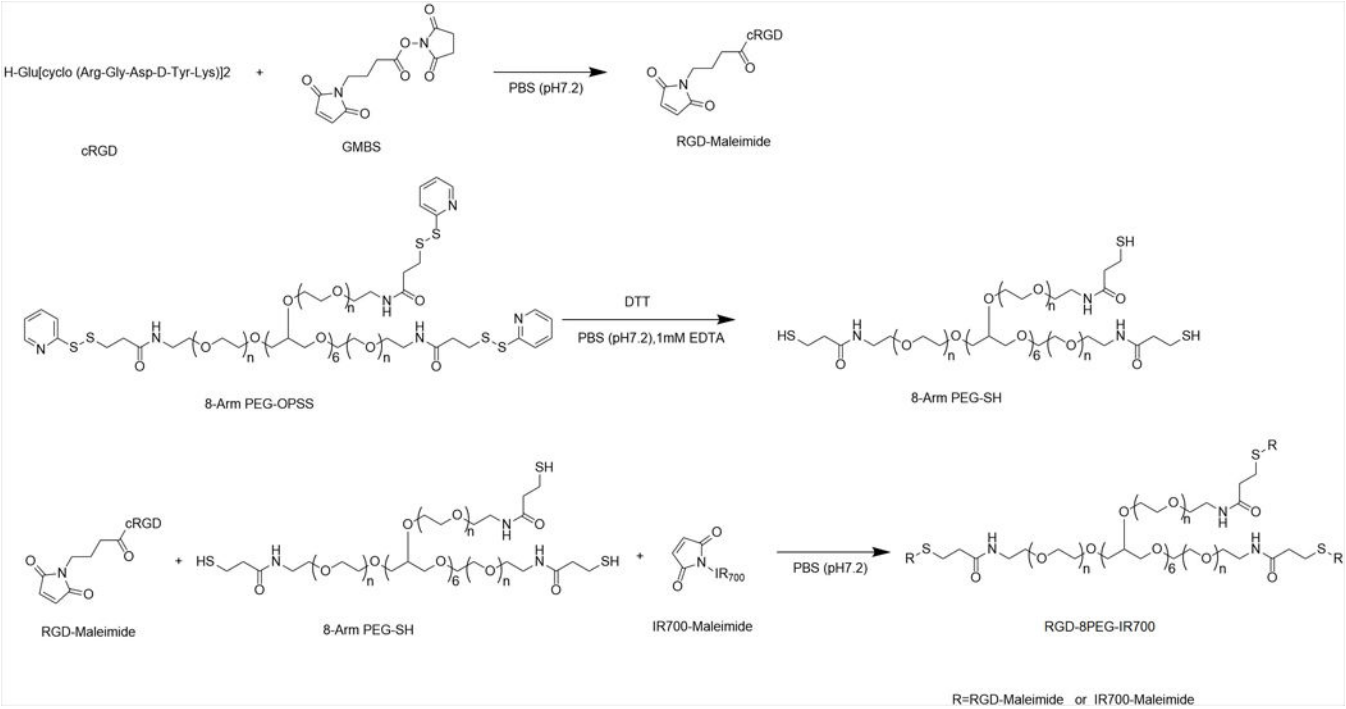

Figure 1.
Scheme of synthesis of RGD-8PEG-IR700 nanoconjugates.

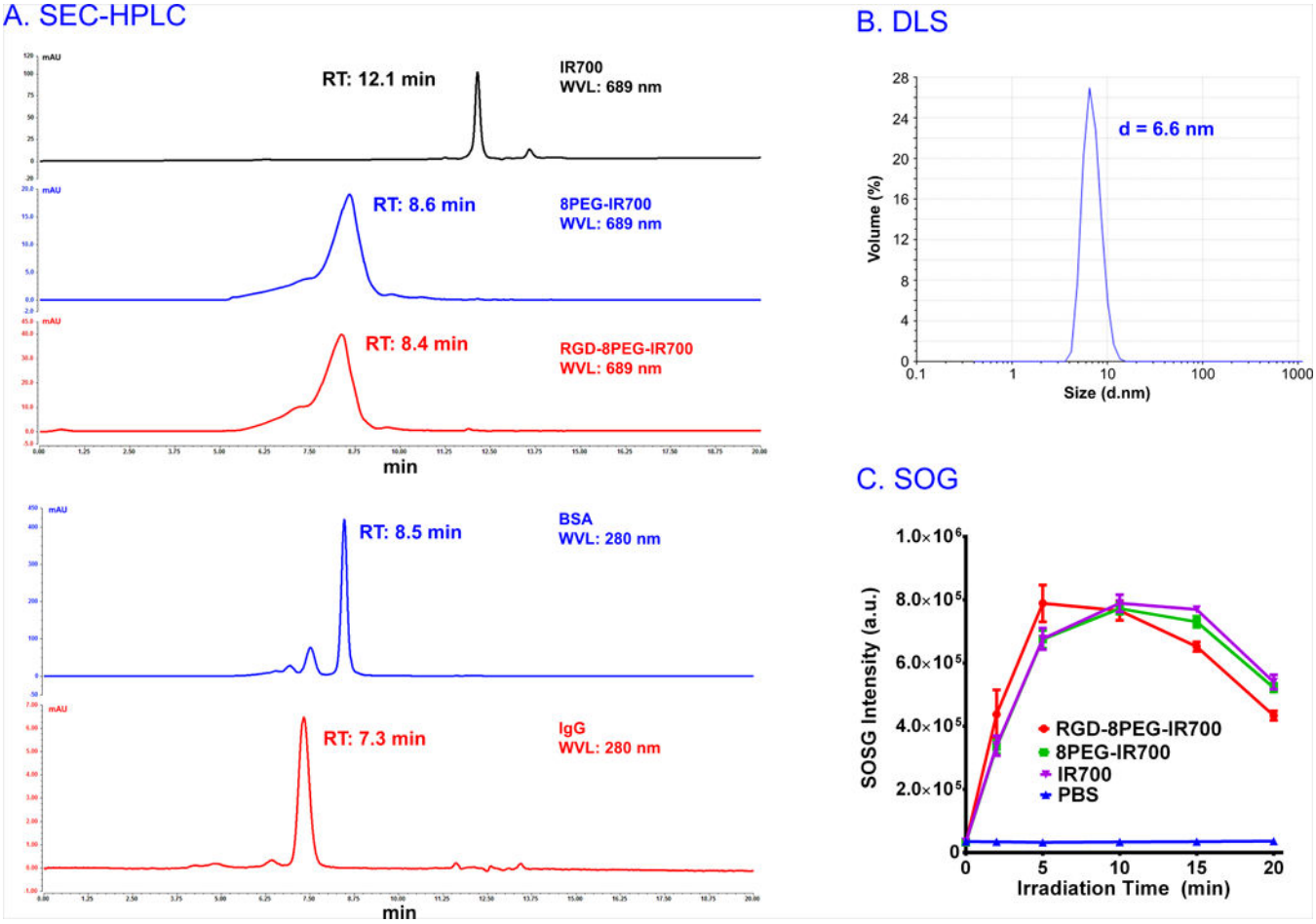

Figure 2.

Physicochemical characterization of nanoconjugates. A. SEC-HPLC chromatography of IR700, 8PEG-IR700 conjugates, and RGD-8PEG-IR700 nanoconjugates (λ = 689 nm), as well as BSA and IgG (λ = 280 nm). B. Particle size distribution of RGD-8PEG-IR700 nanoconjugates determined with DLS. C. Singlet oxygen generation of IR700, 8PEG-IR700, and RGD-8PEG-IR700.

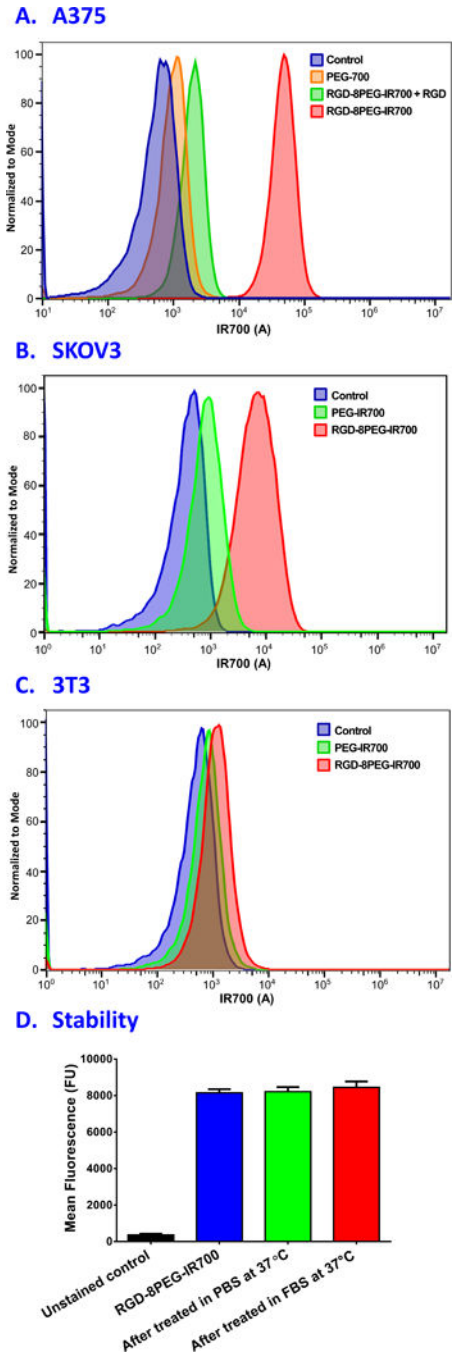

Figure 3.

Cellular uptake and serum stability of nanoconjugates. A. Flow cytometry histogram for cellular uptake of 8PEG-IR700 and RGD-8PEG-IR700 nanoconjugates in the absence and presence of free RGD peptide in A375 cells. B. Flow cytometry histogram for cellular uptake of 8PEG-IR700 and RGD-8PEG-IR700 nanoconjugates in SKOV3 cells. C. Flow cytometry histogram for cellular uptake of 8PEG-IR700 and RGD-8PEG-IR700 nanoconjugates in 3T3 cells. D. Cellular uptake of RGD-8PEG-IR700 after incubation in

PBS or FBS. RGD-8PEG-IR700 was incubated in PBS or 20% FBS at 37 °C for a day, and then their cellular uptake in SKOV3 cells was measured using flow cytometry.

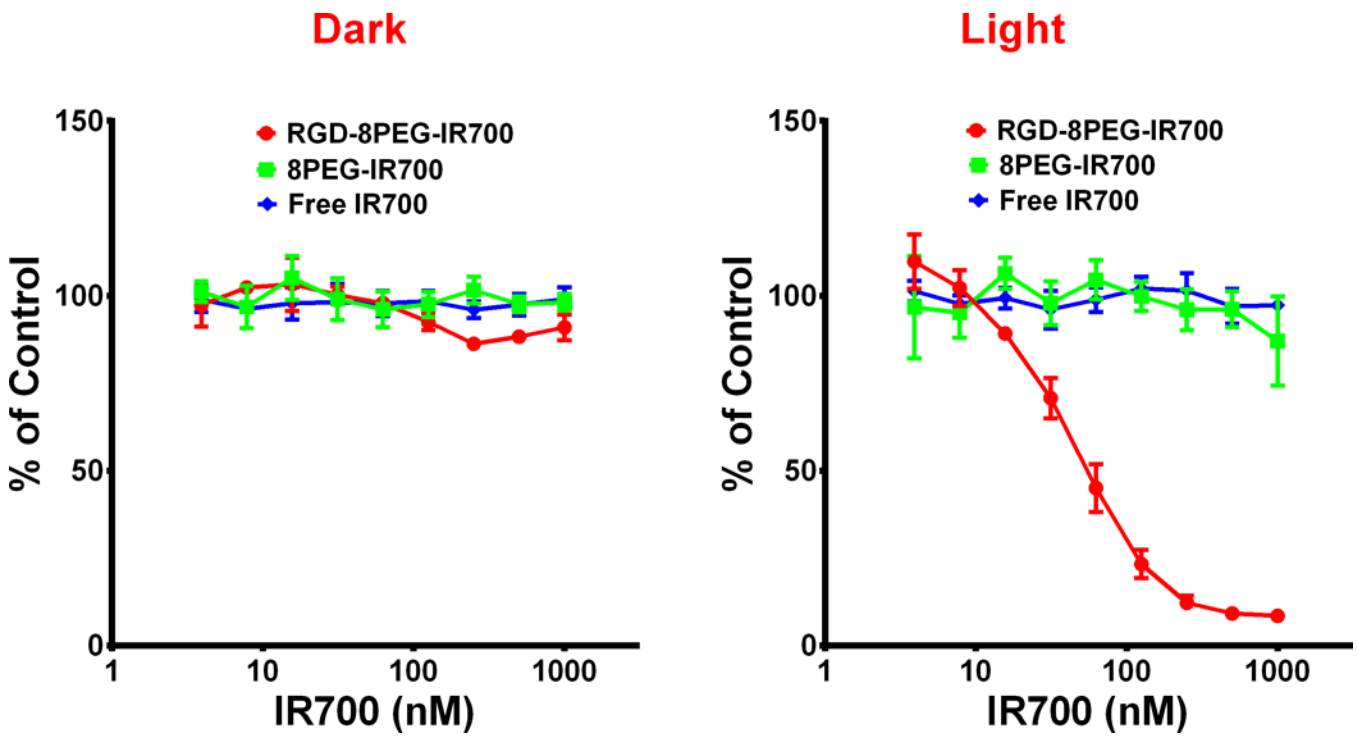

Figure 4.

Dose-dependent phototoxicity of free IR700, 8PEG-IR700 and RGD-8PEG-IR700 in A375 cells. Alamar Blue assay was performed after A375 cells were treated with free IR700, 8PEG-IR700 and RGD-8PEG-IR700 followed by light irradiation (Right). A375 cells that were only treated with PSs served as controls (Left). N = 4.

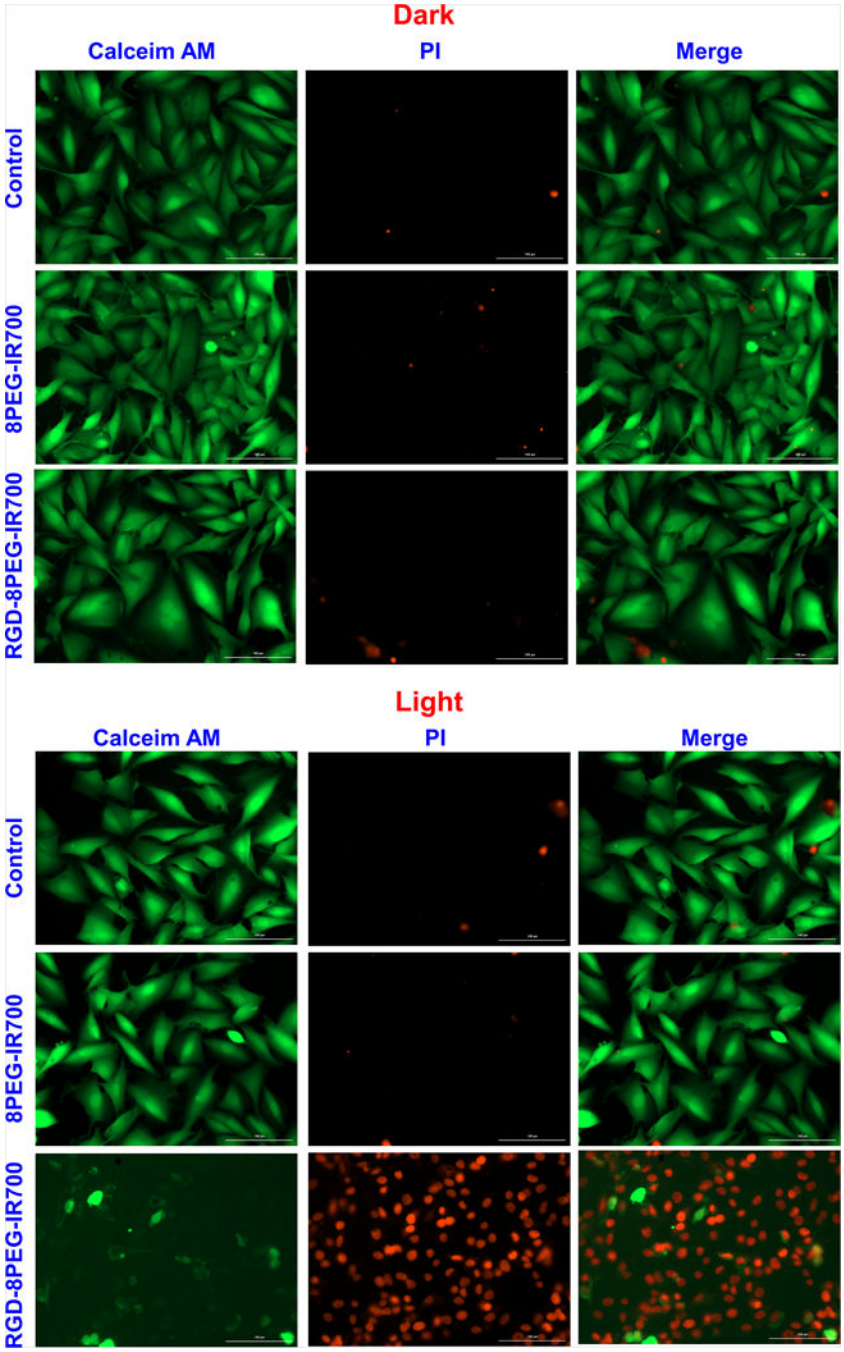

Figure 5.

Live/dead staining of A375 cells after targeted PDT. A375 cells were treated with the 8PEG-IR700 and RGD-8PEG-IR700 nanoconjugates overnight. Live/dead staining was performed after photoirradiation. The cells that were treated with the nanoconjugates but were not irradiated served as control. Scale bar: 100 μm.

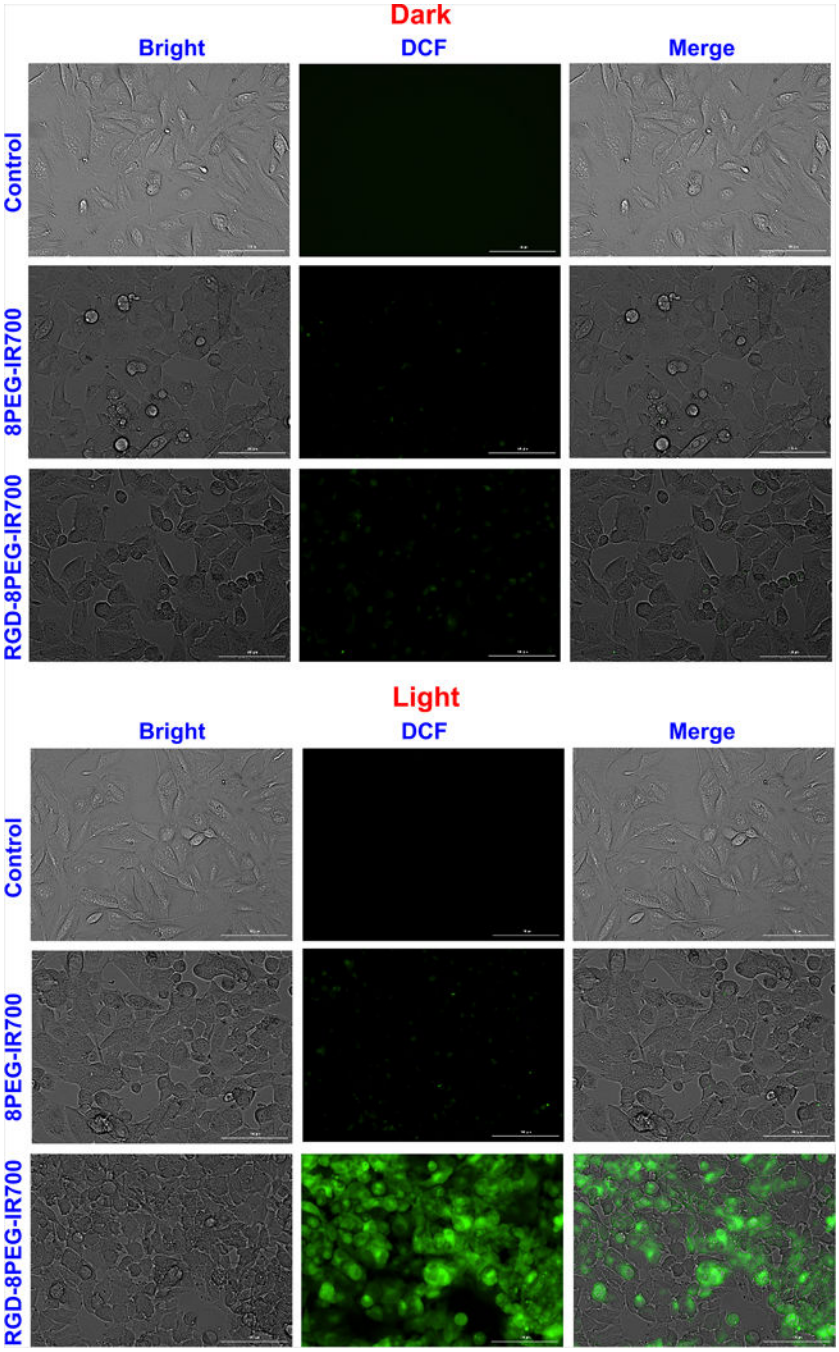

Figure 6.

Intracellular singlet oxygen detection. A375 cells were treated with the nanoconjugates followed by photoirradiation. Fluorescence images of ROS generation were taken using a cellular ROS probe, CM-H_2DCFDA. Scale bar: 100 μm.

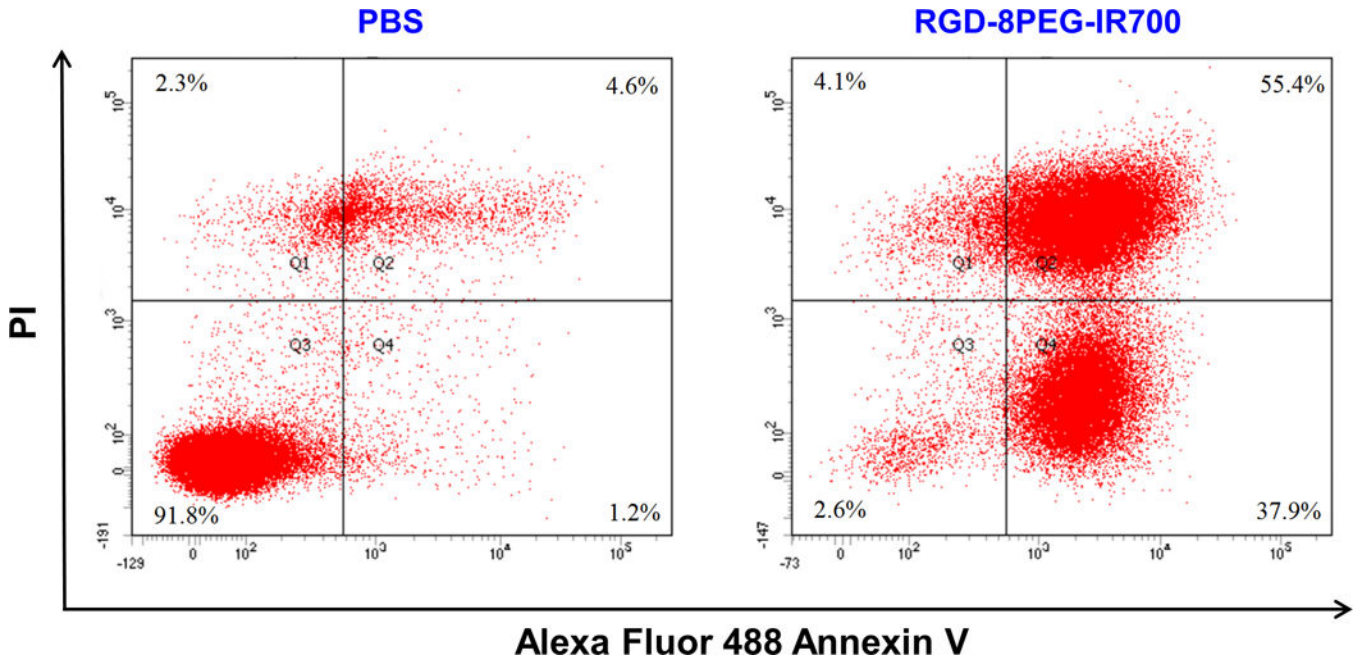

Figure 7.

Flow cytometry analysis of A375 cells cell death induced by RGD-8PEG-IR700 mediated PDT. A375 cells were treated with the nanoconjugates followed by photoirradiation. Flow cytometry analysis was performed after staining with Annexin V/PI.

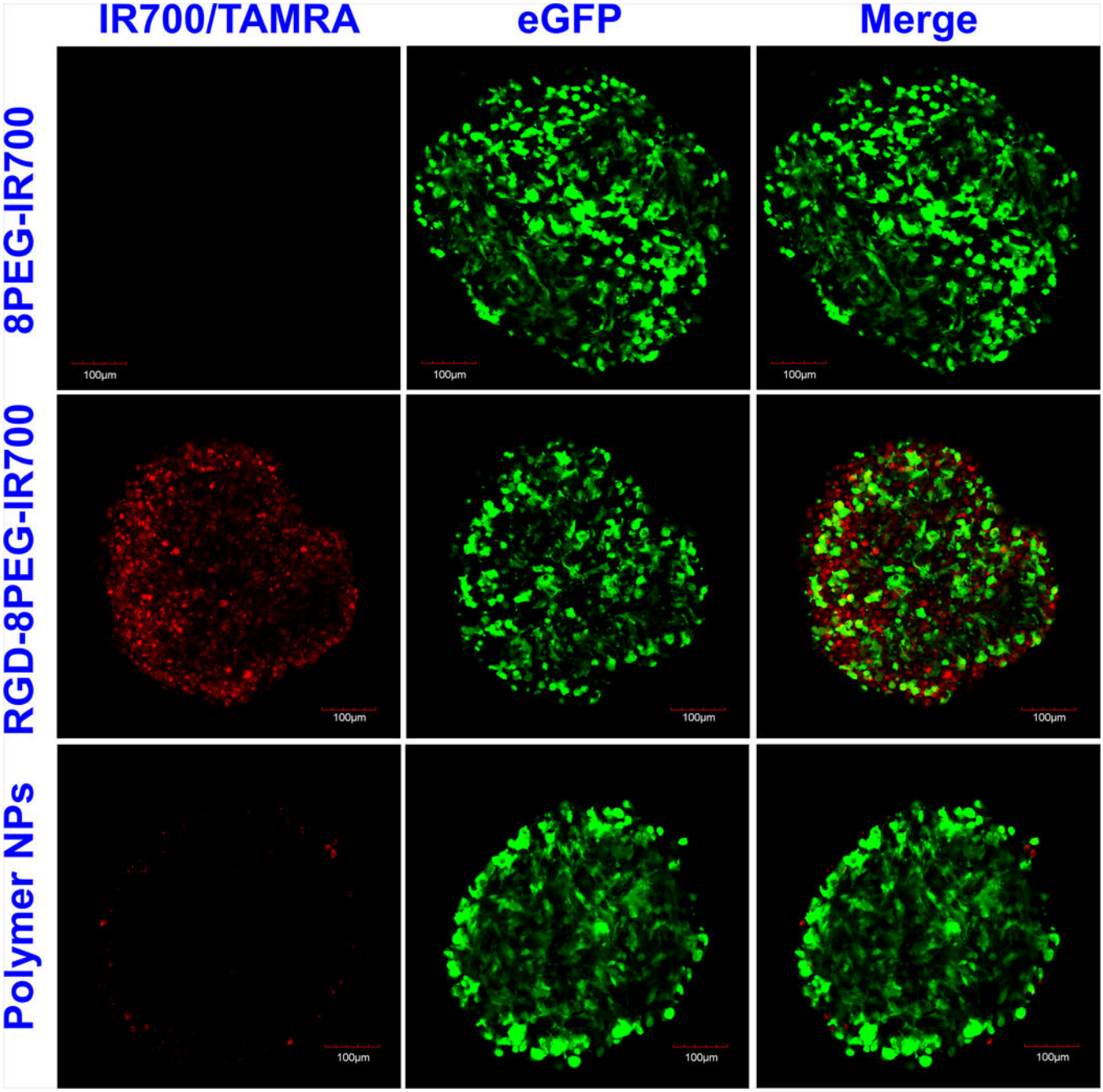

Figure 8.

Penetration of the targeted nanoconjugates in tumor spheroids. Spheroids of A375/GFP cells were treated with 8PEG-IR700, RGD-8PEG-IR700, and polymer NPs for 4h. After washing, the spheroids were observed with confocal microscopy. Green: GFP fluorescence. Red: IR700/TAMRA fluorescence. Scale bar: 100 μm.

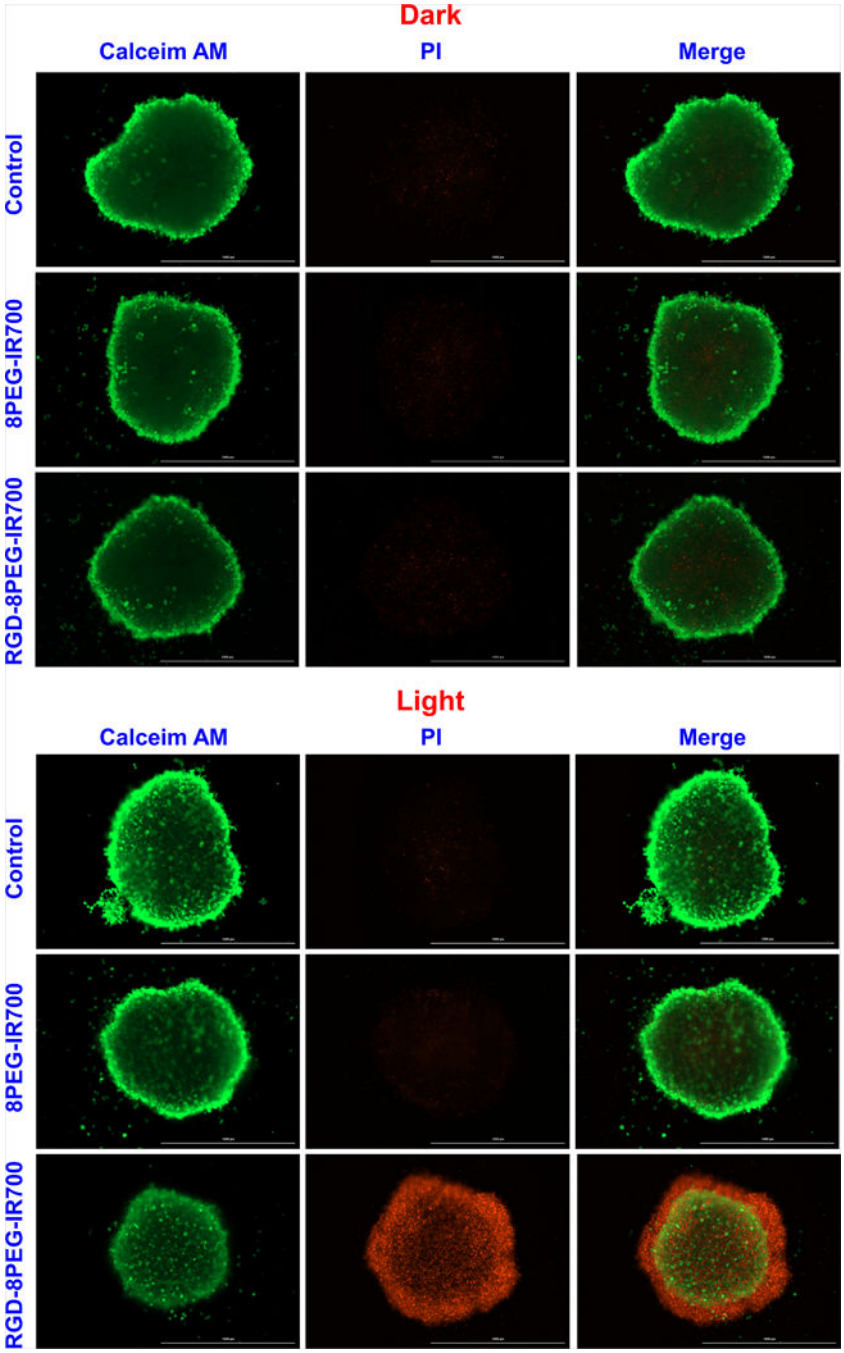

Figure 9.

Live/dead staining of A375 spheroids after PDT with the nanoconjugates. A375 spheroids were treated by 8PEG-IR700 and RGD-8PEG-IR700 overnight. After washing, the spheroids were irradiated with the 660 nm LED light. Live/dead staining of the spheroids with Calcein-AM and PI was performed after 24-h culture. Scale bar: 1000 μm.